Applied Catalysis B: Environmental 181 (2016) 681–691

Contents lists available at ScienceDirect

Applied Catalysis B: Environmental

journal homepage: www.elsevier.com/locate/apcatb

Combustion of textile monoazo, diazo and triazo dyes by solar photoelectro-Fenton: Decolorization, kinetics and degradation routes

Sergi Garcia-Segura, Enric Brillas*

Laboratori d'Electroquímica dels Materials i del Medi Ambient, Departament de Química Física, Facultat de Química, Universitat de Barcelona, Martí i Franquès 1-11, 08028 Barcelona, Spain

ARTICLE INFO

Article history:
Received 22 June 2015
Received in revised form 13 August 2015
Accepted 24 August 2015
Available online 28 August 2015

Keywords:
Acid Orange 7
Acid Red 151
Disperse Blue 71
Solar photoelectro-Fenton
Water treatment

ABSTRACT

The viability of the electrochemical combustion of the monoazo Acid Orange 7, the diazo Acid Red 151 and the triazo Disperse Blue 71 by solar photoelectro-Fenton (SPEF) has been demonstrated. Comparative trials were made by electrolyzing 10 L of 50 mg L^{-1} of dissolved organic carbon of each azo dye in 0.05 M Na_2SO_4 with 0.50 mM Fe^{2+} of pH 3.0 using a solar flow plant equipped with a Pt/air-diffusion filter-press cell coupled to a CPC photoreactor. Organics are oxidized by •OH radicals formed from water oxidation at the Pt anode and in the bulk from the Fenton's reaction between Fe^{2+} and H_2O_2 generated at the cathode, whereas the mineralization was enhanced by the photolysis of intermediates by UV light from sunlight that irradiates the CPC photoreactor. The decay of all the azo dyes was followed by reversed-phase HPLC and always obeyed a pseudo-first-order reaction, being more rapid than the decolorization of the corresponding solutions due to the formation of colored products. The mineralization rate decreased in the order Acid Orange 7 > Disperse Blue 71 > Acid Red 151. Up to 97% mineralization was achieved for the former compound, remaining short-linear carboxylic acids in the final solution. In contrast, 90–92% mineralization was reached for the other two azo dyes and their final solutions contained undetected products more recalcitrant than carboxylic acids. The effect of current density on each degradation process was examined. Similar results were found using either a power supply or a photovoltaic panel to provide the same current density to the cell, corroborating the use of autonomous solar flow plants for SPEF. Aromatic products and hydroxylated derivatives were identified by LCMS and short-linear carboxylic acids were quantified by ion-exclusion HPLC. The formation of SO_4^{2-}, NO_3^- and NH_4^+ ions, along with the loss of volatile N-products, was confirmed by ion chromatography.

1. Introduction

A large variety of dyes are widely used for coloring materials in textile, light-harvesting arrays, pharmaceutical, ink, leather, food, drink, cosmetic and paper industries [1–4]. The most abundant of these compounds are azo dyes, which represent about 70% of the world dye production. Azo dyes are characterized by one or more azo bonds (—N=N—) as chromophore, usually linked to benzenic or naphthalenic rings containing lateral —OH and/or $-SO_3^-$ groups [1,4]. Large volumes of colored wastewater effluents with high levels of azo dyes (between 100 and 250 mg L^{-1}) are daily discharged by many industries throughout the world into water bodies like lakes and rivers. This causes not only aesthetic problems and the hindrance of light penetration in waters, but also health problems on aquatic organism due to the carcinogenicity, toxicity and mutagenicity of azo dyes and their by-products [4,5–8]. The large persistence of azo dyes in the aquatic environment is a result of their resistance to biodegradation and their poor removal by physico-chemical and biological treatments in wastewater treatment plants [5,8]. Research efforts are then needed to develop powerful and effective oxidation methods to destroy these pollutants and their by-products from wastewaters in order to avoid their adverse impact in the environment.

Recently, Fenton based electrochemical advanced oxidation processes (EAOPs) have received increasing attention for water remediation [4,9–11]. The interest of these methods is due to their environmental compatibility, amenability of automation, high energy efficiency, versatility and safety operating at mild conditions. In these EAOPs, H_2O_2 is generated by the two-electron reduction of O_2 gas at a carbonaceous cathode as follows [4]:

$$O_{2(g)} + 2H^+ + 2e^- \rightarrow H_2O_2 \quad (1)$$

* Corresponding author. Tel.: +34 934021223; fax: +34 934021231.
E-mail address: brillas@ub.edu (E. Brillas).

http://dx.doi.org/10.1016/j.apcatb.2015.08.042
0926-3373/

Boron-doped diamond (BDD) [12,13], carbon nanotubes [14,15], graphite [16], activated carbon fiber [17,18], carbon sponge [19], graphite felt [20], carbon felt [21–25] and carbon-polytetrafluoroethylene (PTFE) O_2– or air-diffusion [26–29] electrodes have been utilized for the efficient H_2O_2 production from Reaction (1).

The most ubiquitous Fenton based EAOP is electro-Fenton (EF) in which Fe^{2+} ion is added to the polluted solution to react with generated H_2O_2 via Fenton's Reaction (2) to form Fe^{3+} ion and hydroxyl radical ($^{\bullet}OH$) in the bulk at optimum pH 3. The high standard reduction potential (E° = 2.8 V/SHE) of $^{\bullet}OH$ allows its non-selective reaction with most organics up to mineralization, i.e., conversion into CO_2, water and inorganic ions [19–30]. This radical can act during all the EF treatment because Reaction (2) is propagated from the reduction of Fe^{3+} to Fe^{2+} at the cathode by Reaction (3).

$$H_2O_2 + Fe^{2+} + H^+ \rightarrow Fe^{3+} + H_2O + {}^{\bullet}OH \quad (2)$$

$$Fe^{3+} + e^- \rightarrow Fe^{2+} \quad (3)$$

The use of an undivided cell with a high O_2-overpotential anode (M) in EF makes possible the destruction of organics not only by $^{\bullet}OH$ formed from Fenton's Reaction (2), but also by physisorbed M($^{\bullet}OH$) produced as intermediate from water oxidation by Reaction (4) [31–34]:

$$M + H_2O \rightarrow M({}^{\bullet}OH) + H^+ + e^- \quad (4)$$

The preferred anode in EF is BDD because it yields higher production of reactive BDD($^{\bullet}OH$) than other common anodes like Pt and PbO_2 [35,36], allowing the mineralization of organic contaminants in much larger extent [4,11].

The main limitation of EF in the treatment of azo dyes solutions is the formation of final products like Fe(III)-carboxylate complexes that are very hardly destroyed by generated hydroxyl radicals [4,37,38]. This drawback can be solved by illuminating the solution with an UV radiation supplied by an artificial lamp in the so-called photoelectro-Fenton (PEF) process [11,17,38], which favors: (i) the enhancement of Fe^{2+} regeneration and $^{\bullet}OH$ production by photoreduction of $Fe(OH)^{2+}$, the predominant Fe(III) species at pH ~3.0, from Reaction (5) and (ii) the photodecarboxylation of Fe(III)–carboxylate intermediates from Reaction (6) [39,40]:

$$Fe^{2+} + h\nu \rightarrow Fe^{2+} + {}^{\bullet}OH \quad (5)$$

$$Fe(OOCR)^{2+} + h\nu \rightarrow Fe^{2+} + CO_2 + R^{\bullet} \quad (6)$$

The mineralization of acidic azo dyes solutions becomes even more efficient by using solar PEF (SPEF), involving the irradiation with the potent sunlight as an inexpensive and renewable energy source [37,38]. Our laboratory is interested in developing the SPEF method to show its viability for possible application to industrial scale. In this way, we have recently reported the use of an autonomous solar flow plant to degrade the diazo Direct Yellow 4, which is directly powered by a photovoltaic panel, thereby making the SPEF process more cost-effective [41]. To gain a better knowledge on the applicability of SPEF for azo dyes combustion, we have undertaken a comparative study on the degradation of 10 L of solutions of three typical textile azo dyes, the monoazo Acid Orange 7, the diazo Acid Red 151 and the triazo Disperse Blue 71, with similar aromatics and functional groups, using a flow plant equipped with a Pt/air-diffusion cell coupled with a solar compound parabolic collector (CPC) photoreactor. In this flow plant, Pt was used as the anode instead of BDD because: (i) lower potential differences between electrodes are supplied to the Pt/air-diffusion cell at the same current density (j), thus consuming less electrical energy, and (ii) the powerful degradation action of sunlight minimizes the greater oxidation ability of BDD($^{\bullet}OH$) than Pt($^{\bullet}OH$) [4,41]. For the first time, comparative experiments were performed using a power supply and a photovoltaic panel as energy source to assess the viability of using an autonomous flow plant for SPEF. In previous work [42], we studied the decolorization of solutions of 100 mL with comparative concentrations of these azo dyes by EF in a stirred BDD/air-diffusion tank reactor and it was found that their decolorization rate decreased with increasing the number of azo bonds in the molecule due to the gradual slower reaction with generated hydroxyl radicals.

This paper presents the results obtained for the comparative decolorization, azo dye decay and mineralization of solutions with 50 mg L^{-1} of dissolved organic carbon (DOC) of Acid Orange 7, Acid Red 151 and Disperse Blue 71 in sulfate medium of pH 3 by SPEF using a solar flow plant. Comparative trials were made by providing a constant j either with a power supply or with a photovoltaic panel. The effect of the applied j on their degradation was examined to better clarify the role of generated hydroxyl radicals and sunlight. The decay kinetics for the azo dyes was followed by high-performance liquid chromatography (HPLC), their aromatic intermediates were detected by liquid chromatography–mass spectrometry (LC–MS) and produced short-linear aliphatic carboxylic acids and inorganic ions were quantified by HPLC and ion chromatography, respectively. From these results, a reaction sequence for the initial combustion of each azo dye is finally proposed.

2. Experimental

2.1. Chemicals

Commercial pure Acid Orange 7 and Disperse Blue 71 were purchased from Acros Organics and commercial pure Acid Red 151 was purchased from TCI Europe. Anhydrous sodium sulfate, used as background electrolyte, and iron (II) sulfate heptahydrate, used as catalyst, were of analytical grade from Merck and Fluka, respectively. Carboxylic acids, other chemicals used and organic solvents were either of analytical, LC-MS or HPLC grade supplied by Panreac and Sigma–Aldrich. Solutions were prepared with deionized water and their initial pH was adjusted to 3.0 with analytical grade sulfuric acid from Merck. Standard solutions and mobile phases were prepared with high-purity water obtained from a Millipore Milli-Q system (resistivity >18 MΩ cm at 25 °C).

2.2. Solar flow plant

A sketch of the flow plant built-up by us for the SPEF treatment of azo dyes solutions is shown in Fig. 1. Experiments were carried out with 10 L of 50 mg L^{-1} of DOC of each azo dye in 0.05 M Na_2SO_4 at pH 3.0. Each solution was introduced in the reservoir and recirculated through the plant by means of a magnetic drive centrifugal pump at a liquid flow rate of 200 L h^{-1} regulated by a flowmeter. The solution passed consecutively through the electrochemical reactor, the solar CPC photoreactor and two heat exchangers to maintain the temperature at 35 °C before backing to the reservoir. The electrochemical cell was an undivided filter-press reactor with components of 12 cm × 18 cm in dimension, separated with Viton gaskets to avoid leakages. The anode was a Pt sheet of 99.99% purity purchased from SEMPSA and the cathode was a carbon-PTFE air-diffusion electrode supplied by E-TEK. Both electrodes were of 10 cm × 10 cm in dimension. A PVC compartment with a central window of 9.5 cm × 9.5 cm (90.2 cm^2) was used to contact the effluent with the outer faces of both electrodes separated 1.2 cm. The inner face of the cathode was in contact with a PVC gas chamber where circulated compressed air at a flow rate of 4.5 L min^{-1}, regulated with a back-pressure gauge, for continuous H_2O_2 generation. Electrolyses were performed at constant j provided by either a Grelco GDL3020 power supply or a 50 W

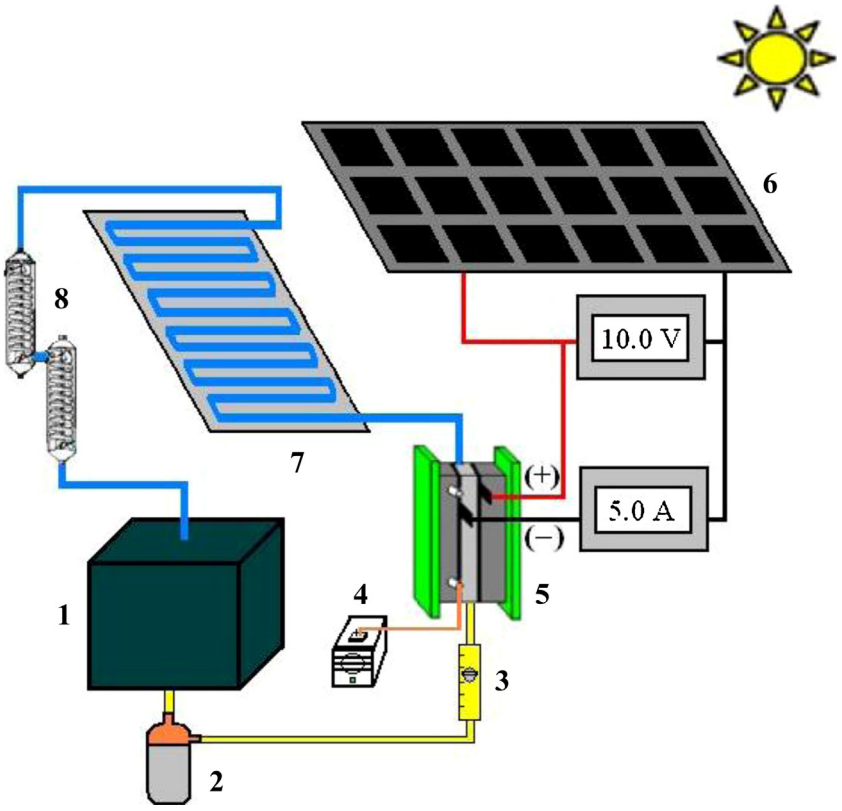

Fig. 1. Sketch of the solar autonomous flow plant used for the solar photoelectro-Fenton (SPEF) treatment of 10 L of azo dyes solutions. (1) Reservoir, (2) magnetic drive centrifugal pump, (3) flowmeter, (4) air pump, (5) electrochemical filter-press reactor with a Pt anode and an air-diffusion cathode of 90.2 cm^2 area, (6) solar photovoltaic panel of 50 W maximum power with the corresponding ammeter and voltmeter, (7) solar compound parabolic components (CPCs) photoreactor of 1.57 L irradiation volume and (8) heat exchangers.

solar photovoltaic panel. The solar CPC photoreactor with a concentration factor of 1 was composed of 12 borosilicate-glass tubes of 50.5 cm length × 1.82 cm inner diameter (1.57 L irradiation volume) mounted in an aluminum frame. Both the solar photovoltaic panel and the CPC photoreactor were placed on separated platforms tilted 41° (local latitude) to better collect the sun rays. The SPEF trials started from noon and were run for 240 min in sunny and clear days during the summer of 2014 at the University of Barcelona, Spain. The average solar UV irradiation intensity between 300 and 400 nm was 30–32 W m^{-2}, as determined with a Kipp&Zonen CUV 5 radiometer. Under these conditions, the photovoltaic panel provided an average current of 5.0 A (j = 55.4 mA cm^{-2}) with an average potential difference between electrodes of 10.0 V. The air-diffusion cathode was previously activated by electrolyzing 10 L of 0.05 M Na_2SO_4 at pH 3.0 and j = 150 mA cm^{-2} for 240 min.

2.3. Apparatus and analytical procedures

The solution pH was measured with a Crison GLP 22 pH-meter. Prior to analysis, the samples withdrawn from electrolyzed solutions were neutralized at pH 7 to stop the degradation process and filtered with 0.45 μm PTFE filters purchased from Whatman. The decolorization of azo dyes solutions was followed from their absorbance (A) decay at the maximum wavelength in the visible region of λ_{max} = 484 nm for Acid Orange 7, λ_{max} = 500 nm for Acid Red 151 and λ_{max} = 584 nm for Disperse Blue 71 [42] using a Shimadzu 1800 UV–vis spectrophotometer thermostated at 35 °C. The mineralization of azo dyes solutions was monitored from the removal of their DOC, measured on a Shimadzu TOC-VCSN analyzer. Reproducible DOC values with ±1% accuracy were found by injecting 50 μL aliquots into the analyzer.

The azo dyes decay was followed by reversed-phase HPLC using a Waters 600 LC fitted with a Spherisorb ODS2 5 μm, 150 mm × 4.6 mm, column at 35 °C and coupled with a Waters 996 photodiode array detector selected at λ = 310 nm for Acid Orange 7, λ = 230 nm for Acid Red 151 and λ = 289 nm for Disperse Blue 71. In these measurements, 20 μL aliquots were injected into the chromatograph using a 30:70 (v/v) acetonitrile/water mixture for Acid Orange 7 and Disperse Blue 71 and a 50:50 (v/v) acetonitrile/water mixture for Acid Red 151, both with 2.4 mM n-butylamine, at 0.6 mL min^{-1} as mobile phase. The recorded chromatograms displayed well-defined absorption peaks with a retention time (t_r) of 7.6 min for Acid Orange 7, 5.4 min for Acid Red 151 and 2.0 min for Disperse Blue 71. The concentration of generated carboxylic acids was determined by ion-exclusion HPLC using the same LC fitted with a Bio-Rad Aminex HPX 87H, 300 mm × 7.8 mm, column at 35 °C and setting the photodiode array detector at λ = 210 nm. These analyses were made by injecting 20 μL aliquots into the LC and using a mobile phase of 4 mM H_2SO_4 at 0.6 mL min^{-1}. The chromatograms displayed well-defined peaks at t_r values of 7.0 min for oxalic acid, 7.9 min for tartronic acid, 8.5 min for tartaric acid, 9.4 min for oxamic acid, 9.5 min for malic acid, 13.4 min for formic acid, 15.1 min for acetic acid and 18.4 min for acrylic acid. NH_4^+, NO_3^- and SO_4^{2-} ions released during azo dyes mineralization were quantified by ion chromatography following the method described elsewhere [41].

The trials were made by triplicate, obtaining good reproducible values. The data given in this work are the mean values found. The figures related to the percentage of color removal, azo dyes decay and TOC removal also show the computed 95% confidence intervals, although in many cases they are included in the experimental symbols.

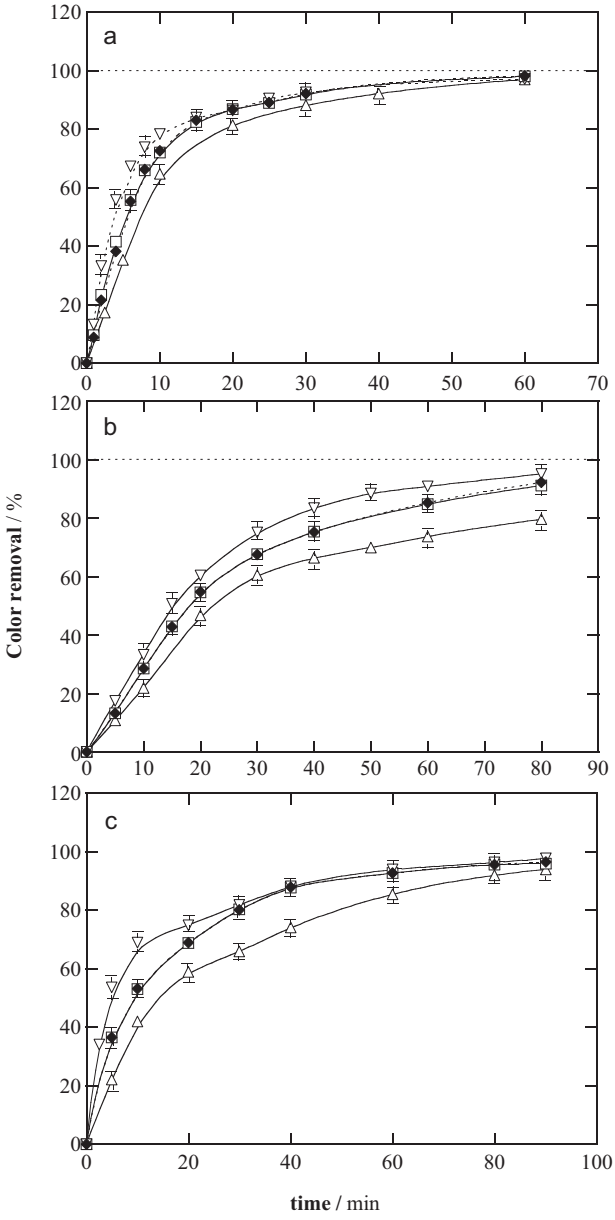

Fig. 2. Change of decolorization efficiency with electrolysis time for the solar photoelectro-Fenton (SPEF) treatment of 10 L of: (a) 0.260 mM Acid Orange 7, (b) 0.190 mM Acid Red 151 and (c) 0.104 mM Disperse Blue 71 in 0.05 M Na_2SO_4 with 0.50 mM Fe^{2+} at pH 3.0 and 35 °C using a flow plant containing a Pt/air-diffusion filter-press reactor of 90.2 cm^2 electrode area coupled with a solar CPC photoreactor of 1.57 L irradiation volume at liquid flow rate of 200 L h^{-1}. Applied current density with a power supply: (Δ) 33.2 mA cm^{-2}, (□) 55.4 mA cm^{-2} and (▽) 77.6 mA cm^{-2}. Applied current density with a photovoltaic panel: (♦) 55.4 mA cm^{-2}.

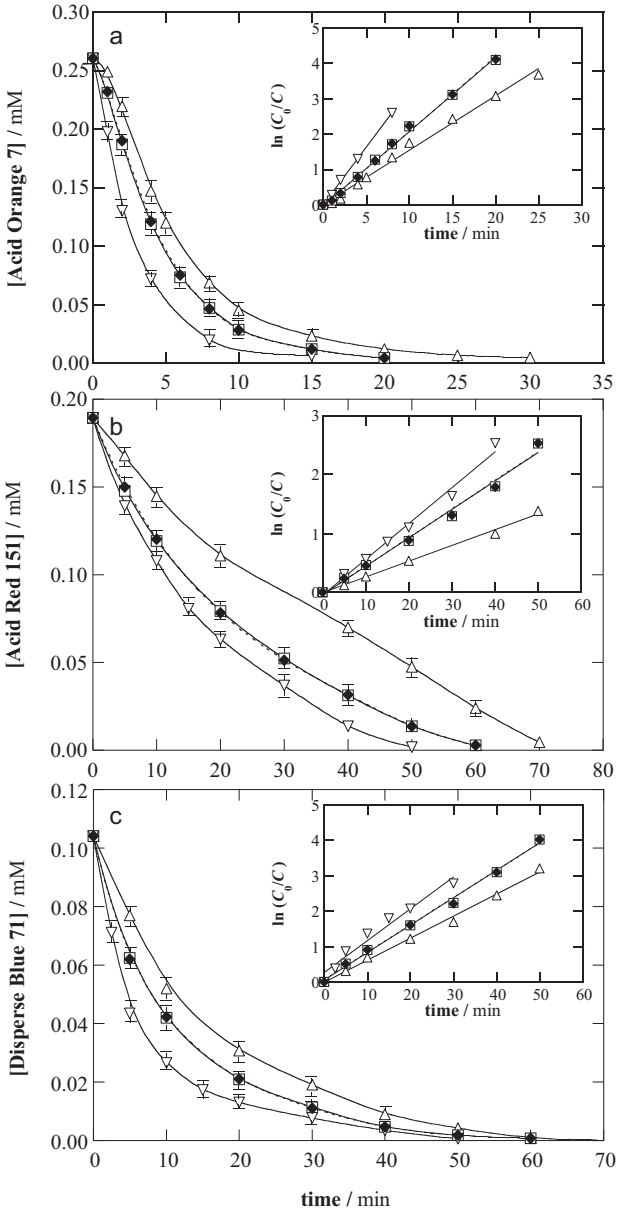

Fig. 3. Decay of azo dye concentration with electrolysis time for the SPEF treatments of Fig. 2. The inset panels present the corresponding kinetic analysis assuming a pseudo-first-order reaction for the azo dye.

Aromatic intermediates formed after 5–60 min of SPEF treatment of 50 mg L^{-1} of DOC of each azo dye solution in the solar flow plant powered by a photovoltaic panel at j = 55.4 mA cm^{-2} were identified by LC–MS using a Shimadzu SIL-20ACLC coupled with a Shimadzu LCMS-2020 MS. The LC was fitted with a Teknokroma Mediterranean Sea C-18 3 μm, 15 mm × 0.46 mm, column at 30 °C. The MS operated in negative mode with electrospray source ionization by applying an interface voltage of −4.5 V and 60 V Q-array RF voltage. The DL temperature was 250 °C and pure N_2 was used as nebulising and dryer gas. Mass spectra were collected using total ion current acquisition mode in the m/z range 55–490 for Acid Orange 7, 55–670 for Acid Red 151 and 55–1280 for Disperse Blue 71. For these analyses, 30 μL aliquots were injected into the LC, previously filtered with a Millipore filter of 0.22 μm, and the mobile phase was a 75:25 (v/v) acetonitrile/water (5.0 mM ammonium acetate) mixture at 0.2 mL min^{-1}.

3. Results and discussion

3.1. Decolorization of azo dyes solutions

Solutions of 50 mg L^{-1} of each azo dye in 0.05 M Na_2SO_4 of pH 3.0 were prepared to be treated by SPEF in the flow plant. A content of 0.50 mM of Fe^{2+} was added as catalyst since it has been found optimal for the treatment of aromatic pollutants in Fenton based EAOPs with an air-diffusion cathode [37,38,41]. Electrolyses were performed by providing a constant j of 33.2, 55.4 and 77.6 mA cm^{-2} with a conventional power supply. Moreover, the trials at an average j of 55.4 mA cm^{-2} were repeated by directly powering the electrolytic cell with a photovoltaic panel to

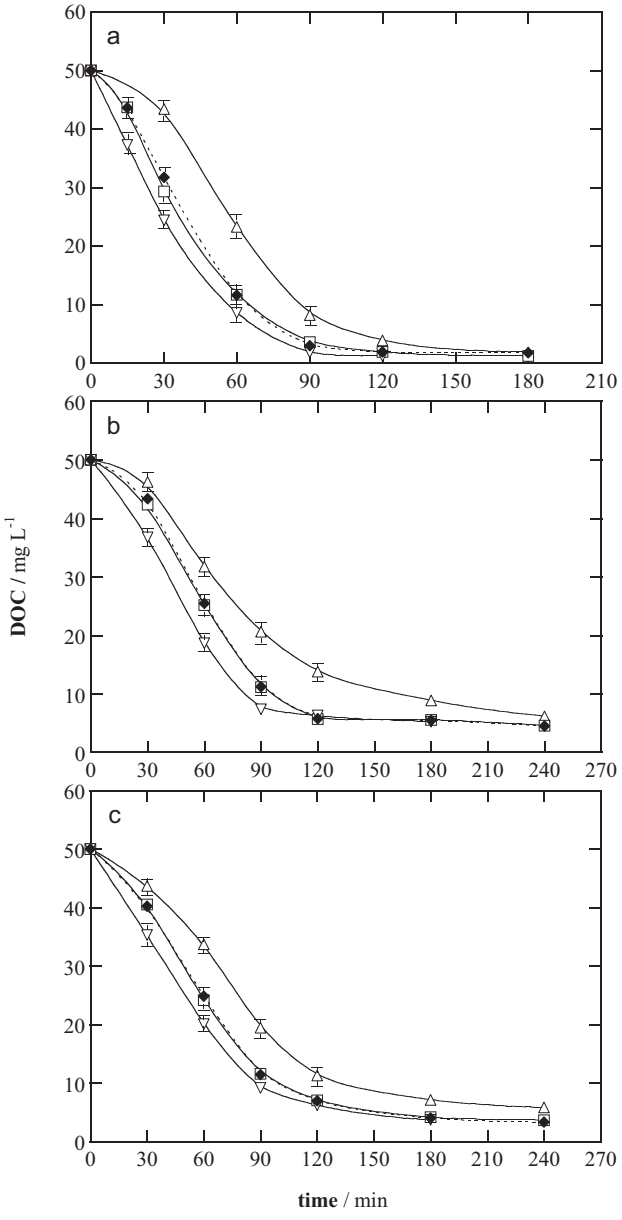

Fig. 4. Variation of DOC with electrolysis time for the trials of Fig. 2. (a) 0.260 mM Acid Orange 7, (b) 0.190 mM Acid Red 151 and (c) 0.104 mM Disperse Blue 71. Applied current density with a power supply: (Δ) 33.2 mA cm^{-2}, (□) 55.4 mA cm^{-2} and (▽) 77.6 mA cm^{-2}. Applied current density with a photovoltaic panel: (♦) 55.4 mA cm^{-2}.

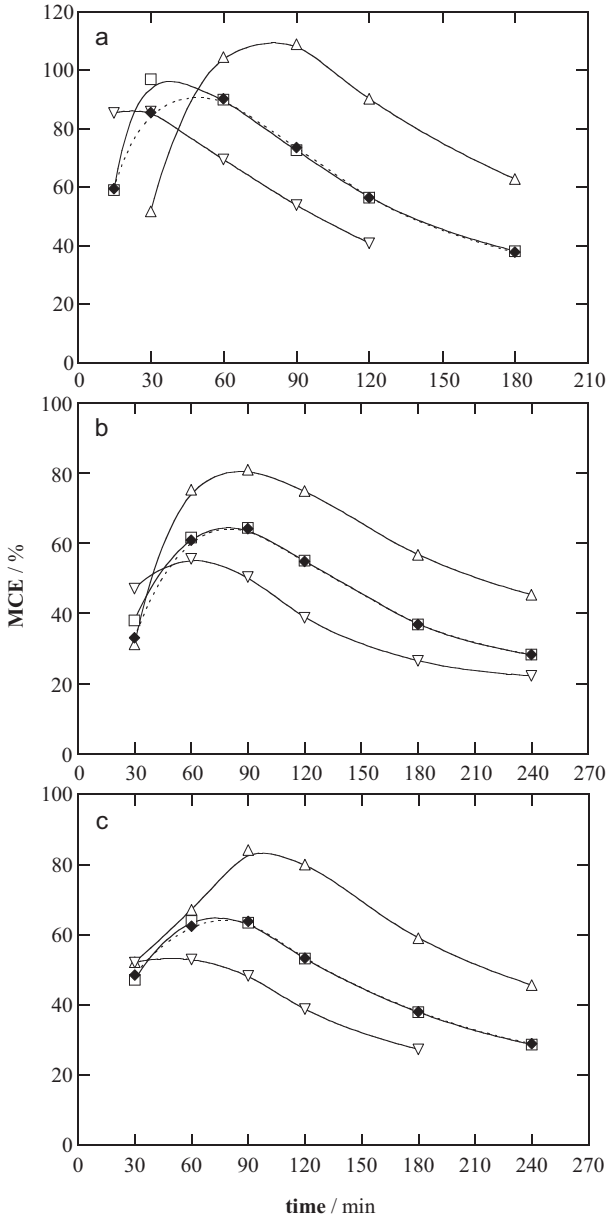

Fig. 5. Mineralization current efficiency calculated from Eq. (11) vs. electrolysis time for the experiments shown in Fig. 4.

demonstrate if its use as electrical energy power is feasible for the flow plant. SPEF experiments were run for 240 min as maximal and in all cases, the initial pH of 3.0 decayed slightly to final values of 2.7–2.8, probably by the formation of acidic products like short-linear aliphatic carboxylic acids [4,11].

Former efforts were concentrated in the determination of the percentage of color removal or decolorization efficiency for the above trials, which was calculated from Eq. (7) [9]:

$$\%\ \text{Color removal} = \frac{A_0 - A_t}{A_0} \times 100 \quad (7)$$

where A_0 and A_t are the absorbance at initial time and time t, respectively, at λ_{max} = 484 nm for Acid Orange 7, λ_{max} = 500 nm for Acid Red 151 and λ_{max} = 584 nm for Disperse Blue 71 [42].

Recirculation of each azo dye solution in the flow plant without passing any current through the electrolytic cell did not yield any color removal, indicating that the starting pollutants were not directly photolyzed by sunlight. When a constant j was applied with a power supply, Fig. 2 highlights a rapid decolorization of all solutions, which rose gradually, but slightly, when j passed from 33.2 to 77.6 mA cm^{-2}. For Acid Orange 7, Fig. 2a shows similar decolorization efficiency at 55.4 and 77.6 mA cm^{-2} for times >15 min and all j values, attaining 97–98% color removal at 60 min. In contrast, a slower decolorization with a much more marked difference with raising j can be observed in Fig. 2b for Acid Red 151, with increasing color removal of 90%, 92% and 95% for growing 33.2, 55.4 and 77.6 mA cm^{-2}. In the case of Disperse Blue 71, Fig. 2c evidences a quicker color removal than that of Acid Red 151 at short electrolysis times, whereas similar decolorization efficiency was also obtained for 55.4 and 77.6 mA cm^{-2} at times >40 min, where the decolorization rate was gradually inhibited to 96–97% at a longer time of 90 min.

The enhancement in decolorization at higher j can be accounted for by the increase in rate of Reaction (4) causing more amount of

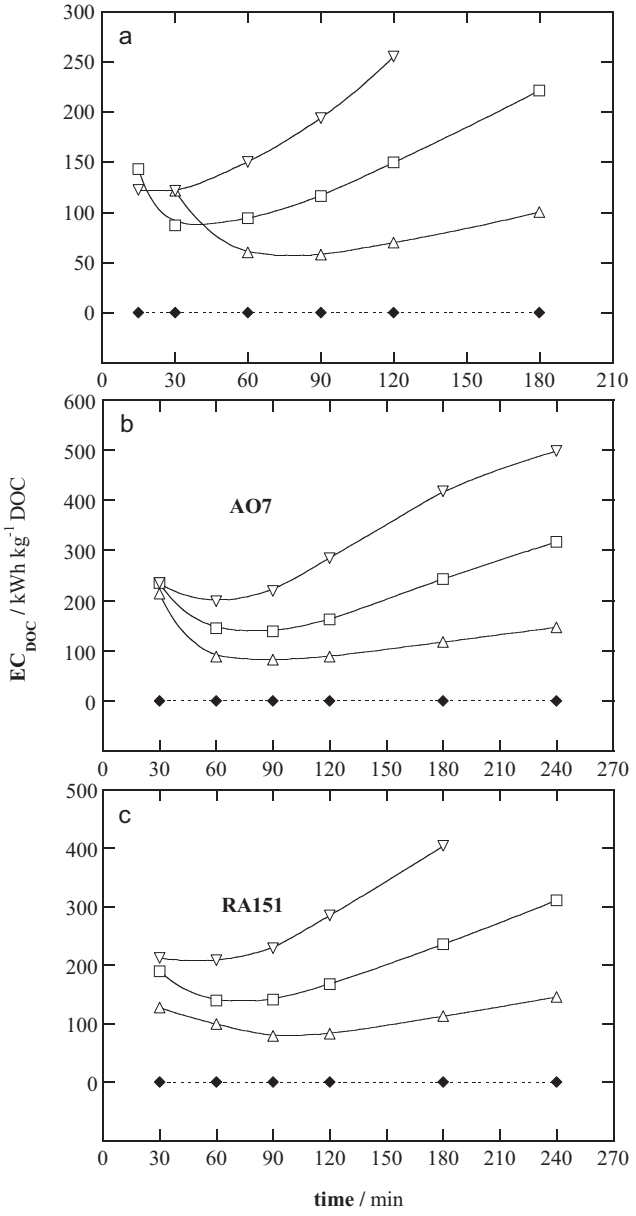

Fig. 6. Specific energy consumption per unit DOC mass removed calculated from Eq. (15) vs. electrolysis time for the trials given in Fig. 4.

Pt(•OH) along with of Reaction (1) yielding greater quantity of H_2O_2 that produces more •OH from Fenton's Reaction (2). The larger production of both hydroxyl radicals, mainly •OH, then accelerates the oxidation of the parent molecules and their colored products that absorb at analogous λ_{max} [4,35]. While this trend is clearly observed for the Acid Red 151 solution, the Acid Orange 7 and Disperse Blue 7 solutions underwent similar color removal at times longer than 10 and 40 min, respectively, for $j \geq 55.4$ mA cm^{-2}, suggesting that their colored oxidation species are more hardly destroyed by both kinds of hydroxyl radicals, thus prolonging the decolorization process. The present results for 50 mg L^{-1} DOC of each azo dye indicate that the solution of the monoazo Acid Orange 7 was the most quickly decolorized, whereas the loss in color removal was generally superior for the triazo Disperse Blue 71 solution compared to that of the diazo Acid Red 151 solution, except at the end of the decolorization processes (see Fig. 2b and c). On the other hand, it is noteworthy that reproducible decolorization efficiencies (with an error <2%) were always obtained at 55.4 mA cm^{-2} when the cell was powered with a photovoltaic panel instead of a power supply, as can be seen in Fig. 2a–c.

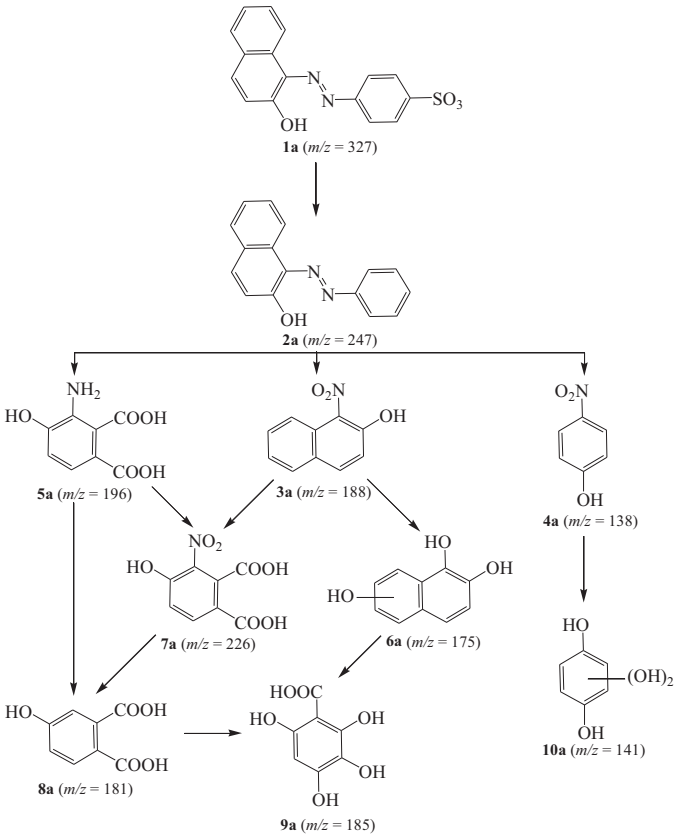

Fig. 7. Proposed reaction pathway for the initial degradation of Acid Orange 7 by SPEF. Intermediates were detected by LC–MS with $z = 1$.

3.2. Kinetics for azo dyes decay

As commented above, the formation of colored products can prolong the decolorization process of azo dyes solutions. To clarify this phenomenon, the decay for the parent molecules was followed by reversed-phase HPLC. Fig. 3a–c depicts the concentration abatement with electrolysis time for the trials of Fig. 2a–c, respectively. As can be seen, the gradual increase in j accelerated the removal of all azo dyes, indicating that they are progressively destroyed by greater amounts of generated hydroxyl radicals, as pointed out above. For Acid Red 151, for example, total disappearance was reached at about 70, 60 and 50 min for 33.2, 55.4 and 77.6 mA cm^{-2}, respectively. Comparison of data of Fig. 3 with those of Fig. 2 allows inferring that each azo dye disappeared much more rapidly than the color of the corresponding solution. This confirms the formation of colored products that are more slowly destroyed with hydroxyl radicals and persisted longer time. Fig. 3 also evidences that the removal of dyes decreased in the order monoazo >triazo >diazo at given j. This seems an abnormal tendency because a slower abatement should be expected for a triazo dye compared with a diazo one at equal concentration [4,42]. However, this requirement is not verified in our case since practically the half concentration of the diazo Acid Red 151 (0.190 mM) was utilized for the triazo Disperse Blue 71 (0.104 mM) trial, thus making more efficient the attack of similar amounts of generated hydroxyl radicals on the lower content of the latter compound.

The above concentration decays were analyzed by means of kinetic equations with simple reaction orders and excellent linear straights were always found considering a pseudo-first-

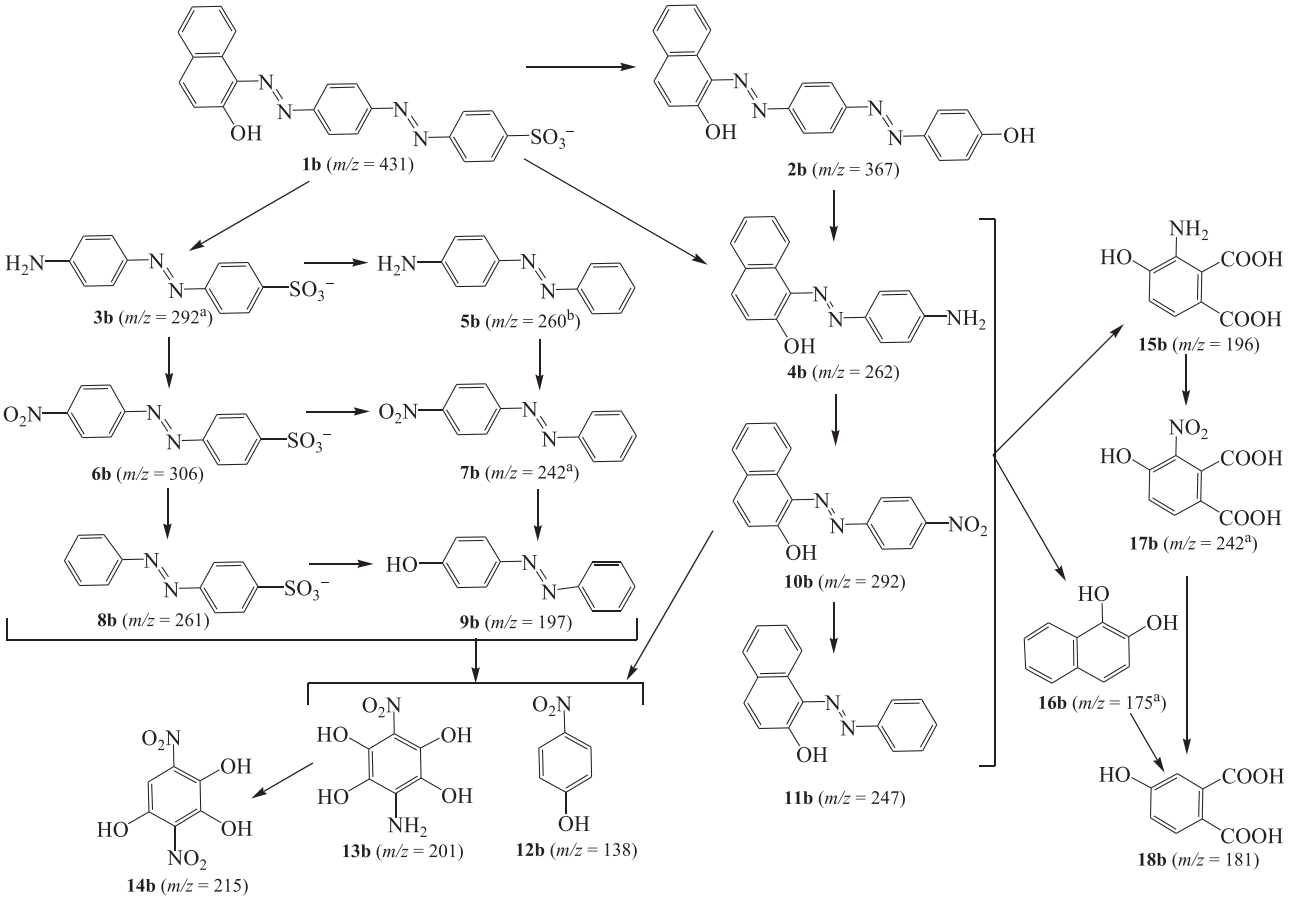

Fig. 8. Reaction sequence proposed for the initial combustion of Acid Red 151 by SPEF. Products were identified by LC–MS with $z = 1$ corresponding to [a]monohydroxylated and [b]tetrahydroxylated derivatives.

order reaction for all the azo dyes, as presented in the inset panels of Fig. 3a–c. For each compound, the apparent rate constant (k_1) became greater with increasing j as expected by its quicker reaction with more amounts of Pt(•OH) and preferentially of •OH produced. Thus, k_1 values of 2.6×10^{-3} s^{-1} ($R^2 = 0.991$) at 33.2 mA cm^{-2}, 3.5×10^{-3} s^{-1} ($R^2 = 0.997$) at 55.4 mA cm^{-2} and 5.4×10^{-3} s^{-1} ($R^2 = 0.9990$) at 77.6 mA cm^{-2} were determined for Acid Orange 7. The corresponding lower k_1 values for Acid Red 151 were 4.5×10^{-4} s^{-1} ($R^2 = 0.995$), 8.0×10^{-4} s^{-1} ($R^2 = 0.990$) and 1.0×10^{-3} s^{-1} ($R^2 = 0.990$), whereas they rose to 1.0×10^{-3} s^{-1} ($R^2 = 0.995$), 1.3×10^{-3} s^{-1} ($R^2 = 0.996$) and 1.5×10^{-3} s^{-1} ($R^2 = 0.985$) for Disperse Blue 71. When the photovoltaic panel was used to power the electrolytic Pt/air-diffusion cell at 55.4 mA cm^{-2}, k_1 values of 3.6×10^{-3} s^{-1} ($R^2 = 0.996$) for Acid Orange 7, 8.1×10^{-3} s^{-1} ($R^2 = 0.996$) for Acid Red 151 and 1.3×10^{-3} s^{-1} ($R^2 = 0.996$) for Disperse Blue 71 were obtained, almost equal to those determined using a power supply. This behavior suggests the presence of a low and quasi-steady concentration of hydroxyl radicals, as a result of their high destruction rate and very short lifetime, to destroy each azo dye, then obeying a pseudo-first-order kinetics.

3.3. Comparative mineralization of azo dyes

The DOC abatement for the SPEF treatments of Fig. 2a–c is shown in Fig. 4a–c, respectively. A greater DOC decay with rising j can be observed for the three azo dyes up to attain an almost constant mineralization at long electrolysis time. This is due to a larger mineralization of intermediates by their oxidation with more quantity of hydroxyl radicals and the consequent acceleration of photocatalytic reactions induced by sunlight on the greater amounts of products formed. Fig. 4a highlights that the DOC of the monoazo Acid Orange 7 solution was gradually reduced by 96% at 180 min of electrolysis at 33.2 mA cm^{-2}, whereas an almost total mineralization of 97% was reached at 180 min of 55.4 mA cm^{-2}, more easily attained at 120 min of 77.6 mA cm^{-2}. In contrast, Fig. 4b shows a slower DOC destruction for the diazo Acid Red 151 solution. While this parameter decreased progressively up to 88% at 240 min of 33.2 mA cm^{-2}, only about 90% mineralization was feasible at times longer than 120 min for $j \geq 55.4$ mA cm^{-2}. Fig. 4c depicts a similar behavior for the triazo Disperse Blue 71 solution, which underwent a DOC removal of 88% at the end of the treatment at 33.2 mA cm^{-2} and of 92% at times ≥180 min for $j \geq 55.4$ mA cm^{-2}. Fig. 4a–c also collects the DOC values for the assays made at 55.4 mA cm^{-2} using the photovoltaic panel, which were always in agreement with those found using a power supply. This fact, along with the almost equal decolorization rates and decay kinetics shown in Figs. 2 and 3 for all the azo dyes using both kinds of power systems, allow concluding that autonomous flow plants powered with photovoltaic panels can be used for the application of the SPEF process, which are necessary, for example, in distant places where the electricity is unavailable.

The aforementioned findings indicate that Acid Orange 7 originates products that can be easily destroyed by hydroxyl radicals and/or the photolytic action of sunlight and hence, it can easily attain an almost total mineralization in short electrolysis time. Conversely, the diazo and triazo dyes form a quite analogous large proportion of final recalcitrant products (about 8–10%) that cannot be removed by generated oxidants and/or sunlight, a phenomenon more apparent operating at $j \geq 55.4$ mA cm^{-2} and that prevents to achieve a more significant mineralization degree.

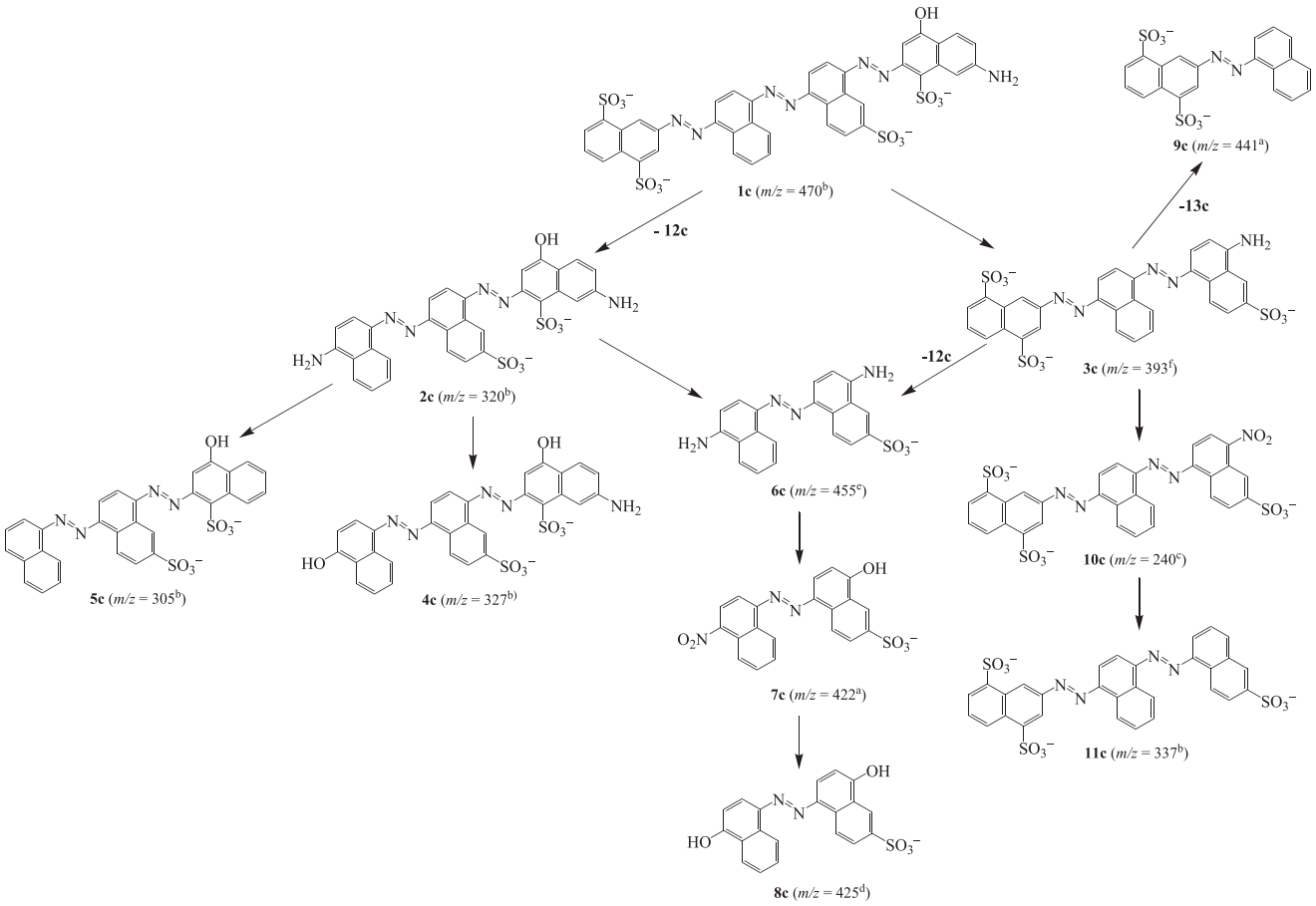

Fig. 9. Proposed oxidation pathway for the conversion of Disperse Blue 71 into diazo and monoazo derivatives. Products were detected by LC–MS with *z*: [a,d–f]1, [b]2 and [c]3. Identified as: [d]dihydroxylated, [e]tetrahydroxylated and [f]hexahydroxylated species.

The inorganic ions produced in the final solutions from the mineralization of the S and N atoms of the azo dyes were quantified by ion chromatography. The S atoms were completely released as SO_4^{2-} ion, with a concentration of 24.85 mg L^{-1} (99.6% of initial S), 18.08 mg L^{-1} (99.1% of initial S) and 39.90 mg L^{-1} (99.9% of initial S) for Acid Orange 7, Acid Red 151 and Disperse Blue 71, respectively. The N atoms were detected as NO_3^- ion along with NH_4^+ ion in minor proportion, but no NO_2^- ion was found. Their concentrations were 17.8 mg L^{-1} of NO_3^- (55.3% of initial N) and 0.98 mg L^{-1} of NH_4^+ (10.4% of initial N) for Acid Orange 7, 18.6 mg L^{-1} of NO_3^- (39.7% of initial N) and 0.77 mg L^{-1} of NH_4^+ (5.7% of initial N) for Acid Red 151 and 17.1 mg L^{-1} of NO_3^- (37.9% of initial N) and 0.28 mg L^{-1} of NH_4^+ (2.1% of initial N) for Disperse Blue 71. That means that 34.3%, 54.6% and 60% of the initial N, respectively, were not mineralized, suggesting that part of such N can remain in the final recalcitrant products and/or it can be lost as volatile N-products, like N_2 and N_xO_y, as proposed for the degradation of other azo dyes by Fenton based EAOPs [4,29,34,41].

From the above results, the theoretical number of electrons consumed per each azo dye molecule (n) for overall mineralization was 84 for Acid Orange 7, 122 for Acid Red 151 and 220 for Disperse Blue 71, considering their conversion into CO_2 with release of NO_3^- and SO_4^{2-} as major inorganic ions, according to Reactions (8)–(10), respectively:

$$C_{16}H_{11}N_2O_4S^- + 38H_2O \rightarrow 16CO_2 + 2NO_3^- + SO_4^{2-} + 87H^+ + 84e^- \quad (8)$$

$$C_{22}H_{15}N_4O_4S^- + 56H_2O \rightarrow 22CO_2 + 4NO_3^- + SO_4^{2-} + 127H^+ + 122e^- \quad (9)$$

$$C_{40}H_{25}N_7O_{13}S_4^{2-} + 104H_2O \rightarrow 40CO_2 + 7NO_3^- + 4SO_4^{2-} + 233H^+ + 220e^- \quad (10)$$

Based on these n-values, the mineralization current efficiency (MCE) for each trial at average current I (in A) and electrolysis time t (in h) was then estimated as follows [37]:

$$MCE(\%) = \frac{nFV_s\Delta(DOC)_{exp}}{4.32 \times 10^7 mIt} \times 100 \quad (11)$$

where F is the Faraday constant (96,487 C mol^{-1}), V_s is the solution volume (10 L), $\Delta(DOC)_{exp}$ is the experimental DOC decay (in mg L^{-1}), 4.32×10^7 is a conversion factor to homogenize units (3600 s h^{-1} × 12,000 mg mol^{-1}) and m is the number of carbon atoms of the azo dye.

Fig. 5a–c presents the corresponding MCE values determined for the experiments ofFig. 4a–c. In all cases, the current efficiency shows a maximum value at short electrolysis time, suggesting the rapid mineralization of easily oxidizable products at the beginning of the SPEF processes, followed by the generation of more recalcitrant products and the loss of organic matter that inhibits the mineralization process and caused the dropping of MCE [31]. A

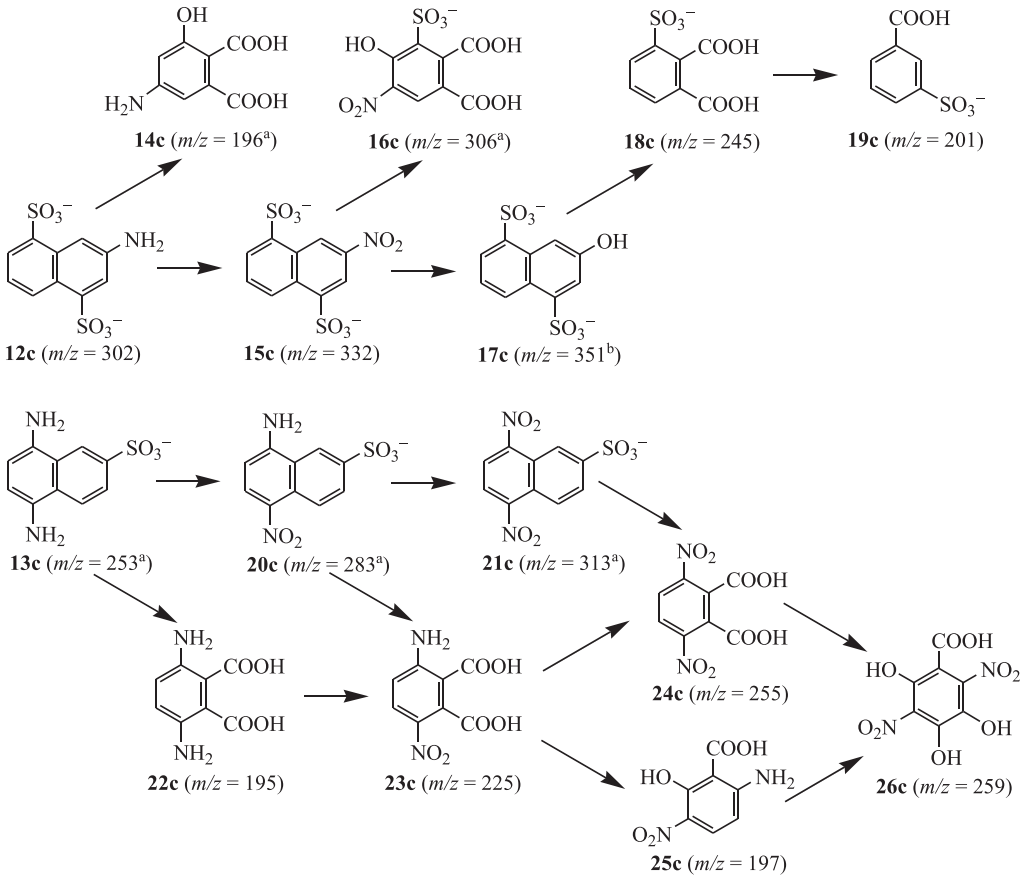

Fig. 10. Proposed evolution of naphthalenic and benzenic derivatives detected by LC–MS with $z = 1$ during the mineralization of Disperse Blue 71 by SPEF. Identified as: [a]monohydroxylated and [b]trihydroxylated products.

look of Fig. 5a–c allows inferring the gradual loss of MCE when j increased for each azo dye, a trend opposite to the greater DOC decay observed in Fig. 4a–c because of the larger production of Pt(•OH) and •OH. This fact is typical of the Fenton based EAOPs and can be accounted for the higher increase in rate of parasitic reactions of both hydroxyl radicals, which progressively diminishes their relative oxidation ability over organic pollutants. These parasitic reactions include, for example, the oxidation of Pt(•OH) to O_2 (in prime) by Reaction (12) as well as the reaction of •OH with Fe^{2+} and H_2O_2 by Reactions (13) and (14), respectively [9,11]:

$$2Pt(^{\bullet}OH) \rightarrow 2Pt + O_2 + 2H^+ + 2e^- \quad (12)$$

$$Fe^{2+} + {}^{\bullet}OH \rightarrow Fe^{3+} + OH^- \quad (13)$$

$$H_2O_2 + {}^{\bullet}OH \rightarrow HO_2^{\bullet} + H_2O \quad (14)$$

Note that the SPEF processes always present high current efficiencies that encourage the use of this EAOP. For example, maximum MCE values of 108% for Acid Orange 7, 81% for Acid Red 151 and 84% for Disperse Blue 71 were found at the lowest j of 33.2 mA cm^{-2}, which dropped to 63%, 45% and 46% at the end of the respective treatments.

Fig. 6a–c depicts the specific energy consumption per unit DOC mass removed (EC_{DOC}) calculated for the above trials from Eq. (15) [37,38]:

$$EC_{DOC}\left(kWh\,kg^{-1}\right) = \frac{1000E_{cell}It}{V_s\Delta(DOC)_{exp}} \quad (15)$$

where E_{cell} is the average potential difference between the anode and cathode (in V) and 1000 is a conversion factor (mg g^{-1}). As can be seen, EC_{DOC} was zero when the photovoltaic panel was utilized to provide a $j = 55.4$ mA cm^{-2} since no external electrical energy was consumed. Using a power supply, however, the EC_{DOC} value increased as prolonging electrolysis and decreased with dropping j, also owing to the fall in E_{cell}. Thus, at the end of the treatments at 33.2 mA cm^{-2} the specific energy consumption was 100, 147 and 145 kWh kg^{-1} DOC for Acid Orange 7, Acid Red 151 and Disperse Blue 71, respectively, which grew up to 255, 485 and 403 kWh kg^{-1} DOC upon 77.6 mA cm^{-2}.

The fast decolorization, quicker azo dyes decay and large mineralization achieved for all the azo dyes by SPEF using the solar flow plant points to the viability of this technology at industrial scale. The application of low j values seems preferable because higher MCE values with lower EC_{DOC} are obtained, although longer time is required to achieve a good mineralization degree.

3.4. Identification of oxidation products and proposal of degradation routes

The solutions of Acid Orange 7 (**1a**), Acid Red 151 (**1b**) and Disperse Blue 71 (**1c**) treated by SPEF in the flow plant using a photovoltaic panel at 55.4 mA cm^{-2} were analyzed by LC–MS to ascertain their main oxidation products. This technique revealed the formation of 9 aromatics (compounds **2a–10a** in Fig. 7) and 14 hydroxylated derivatives (see Table SM-1 in Supplementary material) from **1a**, 17 aromatics (compounds **2b–18b** in Fig. 8) and 18 hydroxylated products (see Table SM-2 in Supplementary material) from **1b** and 25 aromatics (compounds **2c–26c** in Figs. 9 and 10, and 92 hydroxylated and desulfonated derivatives (see Table SM-3 in Supplementary material) from **1c**. The hydroxylated products identified for **1a–c** are expected to absorb at similar wavelengths to their parent molecules and then, they can explain the enlarge-

ment of the decolorization processes in front of azo dyes decay. Figs. 7 and 10 shows the proposed degradation routes for the three azo dyes, where Pt(•OH) and pre-eminently •OH are considered the oxidizing agents.

The reaction sequence for **1a** in Fig. 7 is initiated by its desulfonation to give the monoazo **2a**, which subsequently breaks the —N=N— bond yielding the naphtalenic derivative **3a** and the benzenic products **4a** and **5a**. Further denitration with hydroxylation of **3a** leads to the naphthalene **6a**, whereas the oxidation of one benzenic ring of **3a** forms the phthalic derivative **7a**. Deamination of **5a** and denitration of **7a** give the 4-hydroxyphthalic acid **8a**, which is then hydroxylated to **9a**. The latter product could also be produced from the oxidation of **6a**. Finally, **4a** evolves to **10a** via denitration with hydroxylation.

Fig. 8 depicts that **1b** undergoes either desulfonation to yield the diazo **2b** or the cleavage of one of its —N=N— bonds to form the monoazo derivatives **3b** and **4b**. The latter product could also be generated from the breaking of one azo bond of **2b**. The monoazo **3b** can be either desulfonated to **5b** or nitrified to **6b**, which in turn evolve to the monoazos **7b**–**9b** via nitration, desulfonation, denitration and/or hydroxylation. The monoazo **4b** is then nitrified to **10b**, followed by its denitration to give **11b**. Subsequent oxidation of monoazo derivatives leads to: (i) the nitrobenzene **12b** and the nitro-aminobenzene **13b**, which is nitrified to the dinitrobenzene **14b**, (ii) the phthalic acid derivative **15b**, followed by nitration to yield **17b** that is denitrified to the 4-hydroxyphthalic acid **18b**, and (iii) the naphthodiol **16b**, which can be converted into **18b** as well.

The more complex degradation routes for **1c** are consecutively detailed in Figs. 9 and 10. Fig. 9 depicts the initial cleavage of one extreme—N=N— bond of **1c** to produce the diazo dyes **2c** and **3c**. The formation of **2c** involves the loss of the naphthalenic derivative **12c** (see Fig. 10). Deamination with hydroxylation, di-deamination or breaking of one azo bond of **2c** leads to the diazos **4c** and **5c** or the monoazo **6c**. The latter compound can also be formed from the breaking of one —N=N— bond of **3c** with loss of **12c**. Further nitration of **6c** yields **7c**, which is subsequently denitrified with hydroxylation to yield **8c**. The diazo **3c** can undergo the breaking of one azo bond producing the monoazo **9c** with the release of the naphthalenic compound **13c** (see Fig. 10) or it can be nitrified to **10c**, followed by its denitration to **11c**. On the other hand, Fig. 10 presents the parallel destruction of the released **12c** and **13c**. The former naphthalenic derivative is either oxidized to the phthalic compound **14c** or nitrified to **15c**, which yields **16c** and **17c** via oxidation and denitration with hydroxylation, respectively. The degradation of **17c** produces the 3-sulfonatebenzoic acid **19c** from decarboxylation of the 3-sulfonatephthalic acid **18c**. Similarly, the degradation route of **13c** involves the consecutive nitration of its amino groups to form **20c** and **21c**. The oxidation of these three latter naphthalenes gives the phthalic compounds **22c**, **23c** and **24c**. While the decarboxylation of **23c** yields the carboxylic acid **25c**, degradarion of **21c** can form **24c** as well. Decarboxylation of **24c** and nitration of **25c**, followed by hydroxylation in both cases, produce finally **26c**.

Ion-exclusion HPLC analysis of the treated solutions using the photovoltaic panel to provide 55.4 mA cm^{-2} to the cell of the flow plant revealed the generation of 6 final carboxylic acids from each azo dye. Tartaric, tartronic, malic, acrylic and/or acetic acids proceeded from the cleavage of the aromatic (benzenic and naphthalenic) moieties of intermediates, which were in turn oxidized to oxalic and formic acids [28,29,34,41]. Oxamic acid can be formed from the degradation of N-derivatives. Note that oxalic, oxamic and formic acids are ultimate carboxylic acids that are directly converted into CO_2 [4,11]. Under the present experimental conditions, all the short-linear carboxylic acids formed Fe(III)-carboxylate complexes in large extent, which are expected to react hardly with

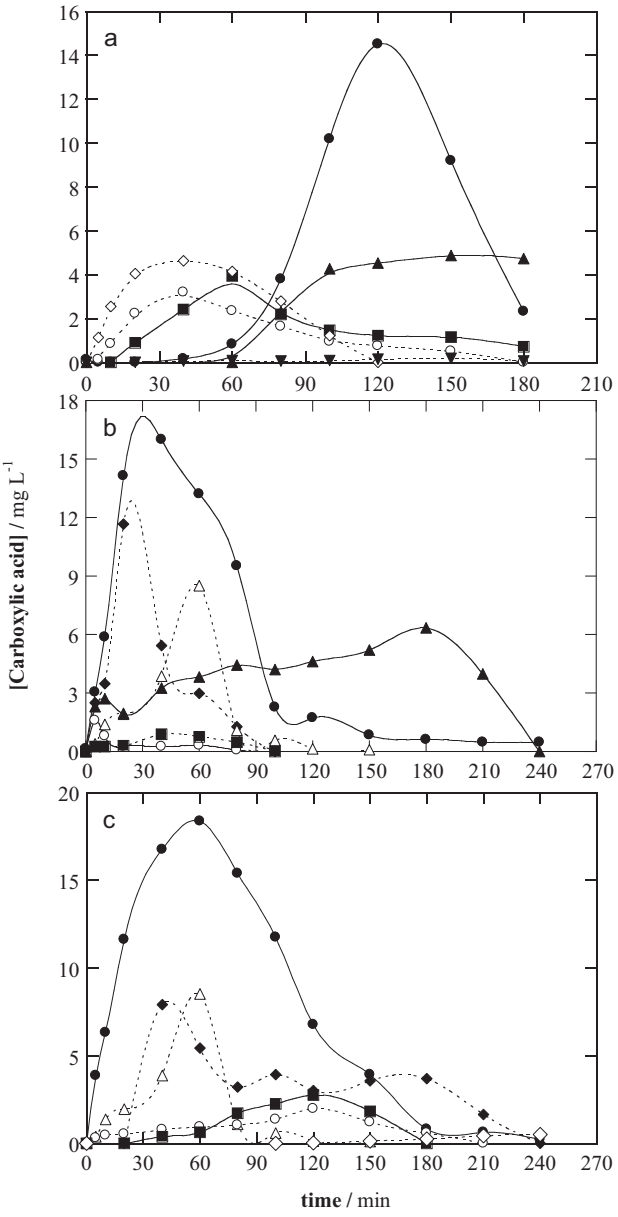

Fig. 11. Time-course of the concentration of: (●) oxalic, (△) acrylic, (♦) malic, (○) tartaric, (▼) oxamic, (■) tartronic, (◊) acetic and (▲) formic acids detected during the SPEF treatment of 10 L of: (a) 0.260 mM Acid Orange 7, (b) 0.190 mM Acid Red 151 and (c) 0.104 mM Disperse Blue 71 using the flow plant powered with a photovoltaic panel at 55.4 mA cm^{-2}.

•OH and/or photodecarboxylated by UV light from sunlight via Reaction (6) [4,9,11].

The time-course of detected carboxylic acids is shown in Fig. 11a–c. In all cases, oxalic acid was the most important final product, attaining a maximum content of 14.5, 16.0 and 18.4 mg L^{-1} for Acid Orange 7, Acid Red 151 and Disperse Blue 71, respectively. However, this acid further disappeared rapidly due to the rapid photolysis of Fe(III)–oxalate complexes [41]. At the end of the treatment of the Acid Orange 7 solution, 0.7 mg L^{-1} of tartronic acid, 2.3 mg L^{-1} of oxalic acid and 4.2 mg L^{-1} of formic acid were detected (see Fig. 11a), which represent 1.8 mg L^{-1} of DOC, i.e., the same DOC as found for the final remaining solution (see Fig. 4a). That means that the Acid Orange 7 solution is finally degraded to short-linear carboxylic acids, whose persistence explains the enlargement of its mineralization. In contrast, Fig. 11b and c evidences that practically no carboxylic acids remained after 240 min of electrolysis, indicating that the 4–5 mg L^{-1} of DOC present in the final solutions of Acid

Red 151 (see Fig. 4b) and Disperse Blue 71 (see Fig. 4c) are due to undetected oxidation products that are even more recalcitrant than final carboxylic acids.

4. Conclusions

It has been shown that the SPEF treatments carried out with a 10 L solar flow plant with a Pt/air-diffusion cell coupled to a CPC photoreactor are viable for the combustion of acidic solutions with 50 mg L^{-1} DOC of textile monoazo, diazo and triazo dyes. The monoazo Acid Orange 7 solution underwent the faster decolorization, azo dye decay and DOC removal, attaining an almost total mineralization with 97% DOC abatement in about 180 min. The diazo Acid Red 151 solution was degraded more slowly than the triazo Disperse Blue 71 one, but in both cases the final solution still contained 8–10% of remaining DOC due to the formation of very recalcitrant products. All the azo dyes always obeyed a pseudo-first-order reaction and their decay was much more rapid than the decolorization process because of the generation of colored products that are more hardly removed by hydroxyl radicals. The increase in j accelerated the destruction of all the pollutants, but caused the drop in MCE and the enhancement of EC_{DOC}. Similar results were obtained using either a power supply or a photovoltaic panel to provide the same j to the electrolytic cell, thus corroborating the use of autonomous solar flow plants for SPEF. From the aromatic products and hydroxylated derivatives identified by LC–MS, the degradation routes for each azo dye have been proposed. Generated carboxylic acids remained as final products of Acid Orange 7 degradation, whereas these compounds were completely destroyed during the combustion of Acid Red 151 and Disperse Blue 71. The initial S of all the starting pollutants was completely converted into SO_4^{2-} ion. In contrast, the initial N was always detected as NO_3^- ion and in minor proportion as NH_4^+ ion, although a large extent of it was lost as volatile N-products.

Acknowledgments

The authors are grateful to MINECO (Ministerio de Economía y Competividad, Spain) for economical support, co-financed with FEDER funds, under project number: CTQ2013-48897-C2-1-R. S. Garcia-Segura thanks the Doctoral grant awarded from MEC (Ministerio de Educación y Ciencia, Spain).

Appendix A. Supplementary data

Supplementary data associated with this article can be found, in the online version, at http://dx.doi.org/10.1016/j.apcatb.2015.08.042.

References

[1] T. Robinson, G. McMullan, R. Marchant, P. Nigam, Biores. Technol. 77 (2001) 247–255.
[2] R. Salazar, E. Brillas, I. Sirés, Appl. Catal. B: Environ. 115–116 (2012) 107–116.
[3] V. Khandegar, A.K. Saroha, J. Environ. Manage. 128 (2013) 949–963.
[4] E. Brillas, C.A. Martínez-Huitle, Appl. Catal. B: Environ. 166–167 (2015) 603–643.
[5] E. Forgacs, T. Cserháti, G. Oros, Environ. Int. 30 (2004) 953–971.
[6] S.M.A.G. Ulson de Souza, E. Forgiarini, A.A. Ulson de Souza, J. Hazard. Mater. 147 (2007) 1073–1078.
[7] K.P. Sharma, S. Sharma, S.P. Sharma, K. Singh, S. Kumar, R. Grover, P.K. Sharma, Chemosphere 69 (2007) 48–54.
[8] A.B. dos Santos, F.J. Cervantes, J.B. van Lier, Bioresour. Technol. 98 (2007) 2369–2385.
[9] E. Brillas, I. Sirés, M.A. Oturan, Chem. Rev. 109 (2009) 6570–6631.
[10] S. Vasudevan, M.A. Oturan, Environ. Chem. Lett. 12 (2014) 97–108.
[11] I. Sirés, E. Brillas, M.A. Oturan, M.A. Rodrigo, M. Panizza, Environ. Sci. Pollut. Res. 21 (2014) 8336–8367.
[12] K. Cruz-González, O. Torres-López, A. García-León, J.L. Guzmán-Mar, L.H. Reyes, A. Hernández-Ramírez, J.M. Peralta-Hernández, Chem. Eng. J. 160 (2010) 199–206.
[13] V.M. Daskalaki, I. Fulgione, Z. Frontistis, L. Rizzo, D. Mantzavinos, Catal. Today 209 (2013) 74–78.
[14] A. Khataee, A. Khataee, M. Fathinia, B. Vahid, S.W. Joo, J. Ind. Eng. Chem. 19 (2013) 1890–1894.
[15] A. Khataee, A. Akbarpour, B. Vahi, J. Taiwan Inst. Chem. Eng. 45 (2014) 930–936.
[16] M. Rivera, M. Pazos, M.A. Sanromán, Desalination 274 (2011) 39–43.
[17] A. Wang, J. Qu, H. Liu, J. Ru, Appl. Catal. B: Environ. 84 (2008) 393–399.
[18] I. Yamanaka, T. Hashimoto, R. Ichihashi, K. Otsuka, Electrochim. Acta 53 (2008) 4824–4832.
[19] N. Daneshvar, S. Aber, V. Vatanpour, M.H. Rasoulifard, J. Electroanal. Chem. 615 (2008) 165–174.
[20] M. Panizza, M.A. Oturan, Electrochim. Acta 56 (2011) 7084–7087.
[21] N. Oturan, E. Brillas, M.A. Oturan, Environ. Chem. Lett. 10 (2012) 165–170.
[22] M.S. Yahya, N. Oturan, K. El Kacemi, M. El Karbane, C.T. Aravindakumar, M.A. Oturan, Chemosphere 117 (2014) 447–454.
[23] A. El-Ghenymy, R.M. Rodríguez, E. Brillas, N. Oturan, M.A. Oturan, Environ. Sci. Pollut. Res. 21 (2014) 8368–8378.
[24] H. Olvera-Vargas, N. Oturan, E. Brillas, D. Buisson, G. Esposito, M.A. Oturan, Chemosphere 117 (2014) 644–651.
[25] F. Sopaj, M.A. Rodrigo, N. Oturan, F.I. Podvorica, J. Pinson, M.A. Oturan, Chem. Eng. J. 262 (2015) 286–294.
[26] C. Flox, J.A. Garrido, R.M. Rodríguez, P.L. Cabot, F. Centellas, C. Arias, E. Brillas, Catal. Today 129 (2007) 29–36.
[27] N. Borràs, R. Oliver, C. Arias, E. Brillas, J. Phys. Chem. A 114 (2010) 6613–6621.
[28] S. Garcia-Segura, J.A. Garrido, R.M. Rodríguez, P.L. Cabot, F. Centellas, C. Arias, E. Brillas, Water Res. 46 (2012) 2067–2076.
[29] X. Florenza, A.M. Sales Solano, F. Centellas, C.A. Martínez-Huitle, E. Brillas, S. Garcia-Segura, Electrochim. Acta 142 (2014) 276–288.
[30] E. Rosales, M. Pazos, M.A. Longo, M.A. Sanromán, Chem. Eng. J. 155 (2009) 62–67.
[31] M. Panizza, G. Cerisola, Chem. Rev. 109 (2009) 6541–6569.
[32] E. Tsantaki, T. Velegraki, A. Katsaounis, D. Mantzavinos, J. Hazard. Mater. 207–208 (2012) 91–96.
[33] M.A. Quiroz, J.L. Sánchez-Salas, S. Reyna, E.R. Bandala, J.M. Peralta-Hernández, C.A. Martínez-Huitle, J. Hazard. Mater. 268 (2014) 6–13.
[34] M.J. Martín de Vidales, S. Barba, C. Sáez, P. Cañizares, M.A. Rodrigo, Electrochim. Acta 140 (2014) 20–26.
[35] L. Ciríaco, C. Anjo, J. Correia, M.J. Pacheco, A. Lopes, Electrochim. Acta 54 (2009) 1464–1472.
[36] E.B. Cavalcanti, S. Garcia-Segura, F. Centellas, E. Brillas, Water Res. 47 (2013) 1803–1815.
[37] E.J. Ruiz, A. Hernández-Ramírez, J.M. Peralta-Hernández, C. Arias, E. Brillas, Chem. Eng. J. 171 (2011) 385–392.
[38] A.M.S. Solano, S. Garcia-Segura, C.A. Martínez-Huitle, E. Brillas, Appl. Catal. B: Environ. 168 (2015) 559–571.
[39] Y. Zuo, J. Hoigne, Environ. Sci. Technol. 26 (1992) 1014–1022.
[40] B.C. Faust, R.G. Zepp, Environ. Sci. Technol. 27 (1993) 2517–2522.
[41] S. Garcia-Segura, E. Brillas, Electrochim. Acta 140 (2014) 384–395.
[42] S. Garcia-Segura, F. Centellas, C. Arias, J.A. Garrido, R.M. Rodríguez, P.L. Cabot, E. Brillas, Electrochim. Acta 58 (2011) 303–311.